Ore Geology Reviews 71 (2015) 191–202

Contents lists available at ScienceDirect

Ore Geology Reviews

journal homepage: www.elsevier.com/locate/oregeorev

Reverse Osmosis contributing to metal zoning in porphyry type deposits: A case study

María S. Japas *, Nora A. Rubinstein, Anabel L.R. Gómez

Consejo Nacional de Investigaciones Científicas y Técnicas, Universidad de Buenos Aires, Departamento de Ciencias Geológicas, Pabellón II, Ciudad Universitaria, C1428EHA Buenos Aires, Argentina

ARTICLE INFO

Article history:
Received 3 January 2015
Received in revised form 11 May 2015
Accepted 14 May 2015
Available online 16 May 2015

Keywords:
Potential-energy gradients
Pressure-sensitive process
Osmotic differentiation
Infiernillo porphyry deposit

ABSTRACT

Representing the main source of copper in the world, porphyry copper deposits have been widely studied. Different models have tried to explain the observed metal zoning, but they did not completely explain it. A Permian Cu–Mo porphyry deposit in the San Rafael Massif in Argentina shows a similar metal zoning pattern to those described elsewhere. However, some particular features depart from the conventional cooling model. Based on data from this deposit and on theoretical background, we present and discuss Reverse Osmosis as a complementary process which could have contributed to porphyry metal zoning during the phyllic stage. The existence of potential-energy gradients and the different relative rejection values for distinct ions make Reverse Osmosis a natural mineral-concentration process. At temperatures corresponding to those of porphyry phyllic halo formation and in presence of a phyllic (clay) membrane, Cu, Ag, Zn and Pb would show a strong osmotic differentiation that could have led to the observed metal zoning.

1. Introduction

Although our knowledge on porphyry deposits was significantly advanced during the last decades, some aspects of porphyry evolution still remain obscure. In part, this is due to multiple factors that could control a porphyry system, but also reproducing the porphyry physicochemical conditions in the laboratory is very difficult. Consequently, there are some disagreements concerning porphyry evolution and also some uncertainties that have not yet been satisfactorily explained (Sillitoe, 2010). One of these discrepancies refers to what controls porphyry metal zoning: traditional models explained it solely as a consequence of cooling (Tosdal and Richards, 2001; Sillitoe, 2010; and references therein). While other researchers consider that cooling may not be the only cause (e.g., Deyell, 2005).

The complex nature of porphyry systems would then indicate that a unique standard model to explain processes leading to metal zoning is likely to be an oversimplification (Hedenquist and Richards, 1998). With this in mind, we will analyze the *Infiernillo* Cu-porphyry deposit as it shows some features that deviate from the traditional cooling model. This deposit, considered as a product of a single hydrothermal system (Gómez and Rubinstein, 2010b; Japas et al., 2013), is a model case that allows to identify the potential contribution of other processes than cooling in constraining the metal zoning. In this way and based on field data and theoretical background, we present and discuss a complementary process that could have contributed to control the metal zoning at the *Infiernillo* deposit during the phyllic stage.

2. Geological setting

The *Infiernillo* deposit is located in the San Rafael Massif, Argentina (Fig. 1A). Precambrian outcrops are scarce in this area and include high grade metamorphic rocks, granites, aplites and pegmatites of Grenvillian age (Cingolani and Varela, 1999). From the Ordovician to the Devonian, carbonate and clastic sediments were deposited and later metamorphosed and successively deformed during the mid–late Ordovician and the late Devonian (Famatinian Orogeny Bordonaro et al., 1996). This was followed by Carboniferous–Lower Permian glacio-marine and continental sedimentary sequence (Espejo and López-Gamundí, 1994).

During the late Paleozoic, there was an active magmatic arc on this proto-margin, part of the Choiyoi Magmatic Cycle that includes two sequences (Kleiman and Japas, 2009; Llambías et al., 1993). The lower Choiyoi sequence (281.4 ± 2.5 up to 264.8 ± 2.3 Ma, Rocha-Campos et al., 2011) consists mainly of andesites and dacitic to low silica rhyolitic ignimbrites with geochemical features that indicate a magmatic arc tectonic setting and a transpressional regime produced by the early Permian San Rafael Orogeny (Kleiman and Japas, 2009; Llambías et al., 1993; and references therein). The upper Choiyoi sequence (264.8 ± 2.3 up to 251.9 ± 2.7 Ma; Rocha-Campos et al., 2011) consists of rhyolitic ignimbrites, andesitic dikes, rhyolitic lava flows, dacitic to rhyolitic subvolcanics, and alkaline basaltic andesites with geochemical characteristics transitional between subduction-related and continental intraplate settings and a transtensional regime after the San Rafael Orogeny (Kleiman and Japas, 2009; Llambías et al., 1993).

* Corresponding author at: Depto. Cs. Geológicas, Pabellón II, Ciudad Universitaria, C1428EHA Buenos Aires, Argentina.
E-mail addresses: msjapas@gl.fcen.uba.ar (M.S. Japas), nora@gl.fcen.uba.ar (N.A. Rubinstein), anabel@gl.fcen.uba.ar (A.L.R. Gómez).

http://dx.doi.org/10.1016/j.oregeorev.2015.05.011
0169-1368/

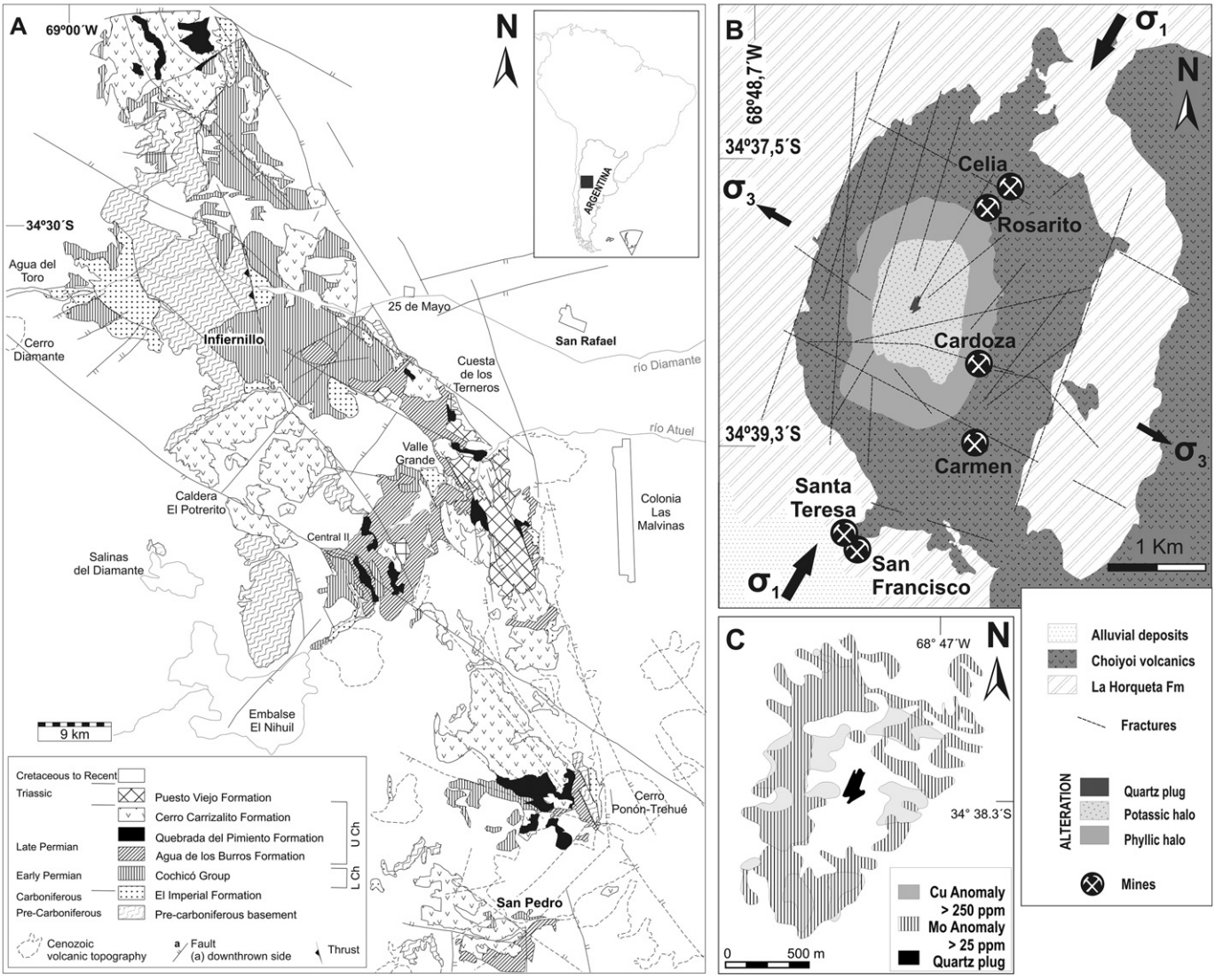

Fig. 1. The *Infiernillo* deposit. A. Location map (modified from Kleiman and Japas, 2009). B. Geology and alteration map. Polymetallic veins are represented as their corresponding mines (after Rubinstein et al., 2013 and Japas et al., 2013). C. Cu and Mo anomaly map (after Fuschini, 1968). Anomalies are located in the inner side of the phyllic halo (Di Tommaso and Rubinstein, 2007).

The main ore deposits in the San Rafael Massif have been linked to the Choiyoi volcanism (Carpio et al., 2001; Rubinstein et al., 2004). Several Cu–(Mo) porphyry type deposits are hosted and genetically linked with the lower Choiyoi (Fuschini, 1968; Gómez and Rubinstein, 2010a, b; Rubinstein et al., 2000, 2012). Genetically related to the upper Choiyoi, there are Mo-porphyry type deposits (Carpio et al., 2001) and epithermal low-sulfidation type deposits (Gargiulo et al., 2007; Rubinstein and Gargiulo, 2005). The different mineralization styles in the upper and lower sections of the Choiyoi Magmatic Cycle were linked to the evolution of the Permian magmatism under a changing tectonic regime (Carpio et al., 2001).

This Permian magmatism was followed by Triassic volcano-sedimentary synrift sequences (Kleiman and Salvarredi, 2001). The geological record from the Upper Cretaceous to Pliocene sequences shows presence of continental sedimentary rocks, as well as volcanic-arc and back-arc products, including felsic to basaltic pyroclastic and volcanic rocks, which were deformed during different phases of the late Cretaceous to present-day Andean Orogeny. Back-arc basaltic volcanism and sedimentation continued from the Pliocene to the Pleistocene (Bermúdez et al., 1993).

3. The *Infiernillo* porphyry deposit

The *Infiernillo* deposit is a Middle Permian Cu–Mo porphyry genetically linked to the lower Choiyoi volcanism (Japas et al., 2013; Fig. 1B) that was emplaced under a waning transpressional regime during the San Rafael Orogeny (Japas et al., 2013). It is hosted by lower Choiyoi highly-welded rhyolitic tuffs that locally show pseudo-flow-banding structures. They are composed of plagioclase, biotite and minor K-feldspar and amphibole crystaloclasts in a recrystallized matrix, with a felsitic texture where fiamme and shards are occasionally recognizable. The NNE-trending alteration zone is of elliptical shape and displays a set of typical concentric halos (Di Tommaso and Rubinstein, 2007; Fig. 1B). The inner potassic alteration zone consists of pervasive K-feldspathization, silicification and minor biotitization and a quartz stockwork. It is surrounded by a halo of pervasive phyllic alteration consisting of quartz, illite (moderately to high crystallinity illite, see Di Tommaso and Rubinstein, 2007) and pyrite with quartz (± pyrite) and pyrite veins.

Surface geochemistry reveals nearly coincident anomalies of Cu and Mo located at the inner border of the phyllic halo (Di Tommaso and Rubinstein, 2007; Fuschini, 1968; Fig. 1C). In the center of the potassic

halo is the hydrothermal breccia composed of silicified host rock fragments cemented by two silicification stages: the first one consists of quartz crystal aggregates and the second one is made up of quartz with textures typical of epithermal deposits (crustiform, cockade, comb, zonal, feathery and flamboyant).

Polymetallic D type veins (according to the classification of Gustafson and Hunt, 1975) with an assemblage of pyrite–chalcopyrite–sphalerite–galena (± arsenopyrite ± electrum ± Ag–tetrahedrite) crop out within or surround the phyllic halo (Fig. 1B) and developed a phyllic envelope with minor veinlets of illite, quartz and pyrite (Gómez and Rubinstein, 2010b).

A late carbonatization process occurred mainly as veins, but also pervasively, overprinting the potassic and phyllic alteration (Di Tommaso and Rubinstein, 2007).

Fluid inclusions studies by Korzeniewski (2012) reveal that during the potassic stage the hydrothermal solutions evolved from early hypersaline brines with high homogenization temperatures (>550 °C) and salinities (40–55 wt.% NaCl eq.) to Cu-bearing brines with lower temperatures (550–390 °C) and salinities (35–47 wt.% NaCl eq.) and late barren fluids with slightly lower temperatures (475–350 °C) and salinities (30–40 wt.% NaCl eq.). During the phyllic stage these brines evolved at lower temperature (335–210 °C) and variable salinities (0.5–20 wt.% NaCl eq.) hydrothermal fluids.

Although sharing common alteration features with classical porphyry architecture (e.g., Lowell and Gilbert, 1970), the *Infiernillo* deposit shows some significant differences due to presence of a central quartz breccia with epithermal textures, and the asymmetry of some physico-chemical features of the phyllic halo. Isocon analyses performed by Rubinstein et al. (2013) revealed a minimum mass increase in the southwestern and southeastern areas (6–8%) and a maximum mass increase in the western sector (26%) of the halo. Furthermore, phyllic compared to potassic alteration shows a general gain in Si–Fe–Al–Mg–K (only weak local depletion in Al in the western zone), loss in Na, and local loss in Mn–Ca in southwestern and western areas (Fig. 2A). At these southwestern and western areas, a well developed stockwork structure is also present.

Concerning metal zoning, the *Infiernillo* deposit shows the most intense Cu and Mo anomalies at the inner border of the phyllic halo (Figs. 1C and 2B), the highest volume percentage of pyrite within this halo and polymetallic veins located within or outwards the phyllic halo (Di Tommaso and Rubinstein, 2007; Fig. 1B). All these features are typical of the classic porphyry deposit model. However, some peculiar features were also recognized (Gómez and Rubinstein, 2010b) such as: a) highest Cu and Mo anomalies in the southwestern part of the phyllic halo (Fig. 2B); b) presence of scarce polymetallic veins in the eastern sector of the phyllic halo and the lack of veins in the western area of this halo (Fig. 1B); c) higher Mo and lower Ag–Zn–Pb contents in the veins in the phyllic halo than those in the peripheral veins; and d) heterogeneous metals distribution in all polymetallic veins (Fig. 2B). It is noteworthy that none of these features could be explained through a simple cooling process because a more symmetric pattern should be expected.

4. Metal zoning and physico-chemical gradients

Porphyry systems are complex systems that are constrained by several competing physical and chemical factors. Besides the most commonly considered factors of temperature, pressure, fluid composition, physical and chemical properties of host rocks, differential stress and also strain rate (Fournier, 1999; Hedenquist and Richards, 1998; Sillitoe, 2010; Tosdal and Richards, 2001), some other important factors concerning solute–solvent interactions appear to be underestimated. These may include thermal-, pressure-, chemical-, pH-, redox- and ionic strength-gradients. Consequently, little attention has been paid to the significance of potential-energy gradients during porphyry evolution.

The vein types and crosscutting relationships (Gómez, 2008) allow to consider that the main metal zoning at the *Infiernillo* deposit had to be produced during the phyllic stage. Regardless of the origin of the *Infiernillo* phyllic halo, it appears to be significant during ore deposition since metal anomalies are distributed around and close to it. Moreover, the *Infiernillo* phyllic halo bounds two regions with contrasting physico-chemical conditions (inside, fluids with high salinity/temperature; outside, fluids with low salinity/temperature) and different pressure conditions (inside, relatively high fluid-pressure/differential-stress ratio; outside, dominant tectonic pressure; Japas et al., 2013).

Some of the phyllic-forming minerals are illite and minor kaolinite (Di Tommaso and Rubinstein, 2007). As these minerals are clays, the inception of this halo should have introduced some modifications into the hydrothermal system. When placed between two solutions with different solute concentrations some clay minerals can act as semi-permeable barriers, also known as “membranes” (Fritz, 1986; Fritz and Marine, 1983; Garavito Rojas, 2006; Marine and Fritz, 1978). “Semi-permeable” means that they act as permeable to water but impervious to the solute.

Membrane processes were empirically considered as probable ore-forming mechanisms at relatively low temperatures (Hart, 2012; MacKay, 1946; Pirajno, 2009; Spirakis, 1977; Whitworth and DeRosa, 1997). Membrane separation systems are generally grouped for industry purposes into five categories: particle filtration (PF), microfiltration (MF), ultrafiltration (UF), nanofiltration (NF), and hyperfiltration or Reverse Osmosis (Fig. 3). The former three (PF, MF, UF) function as purely size exclusion processes based on membrane pore size whereas the latter two (NF, RO) are osmotic processes and therefore they are also conditioned by diffusion.

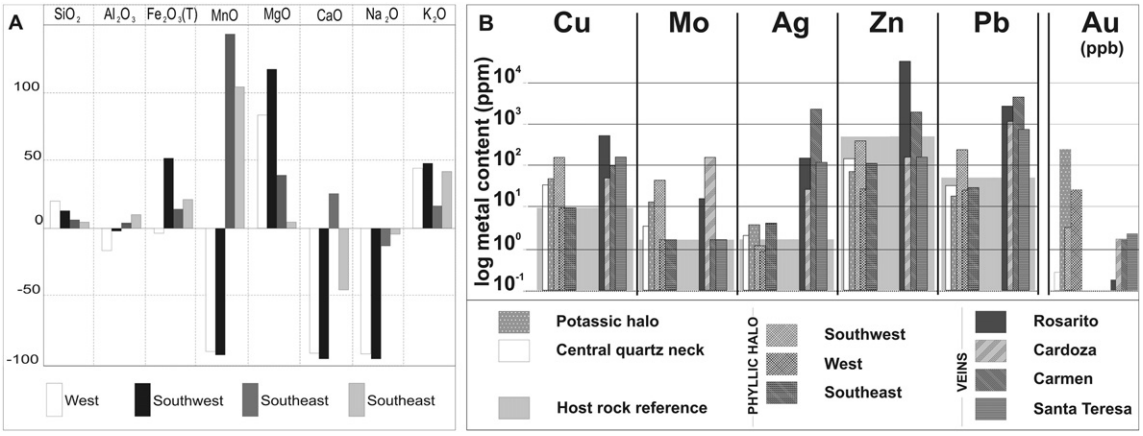

Fig. 2. *Infiernillo* deposit features. A. Phyllic alteration: Percentage of gains and losses for some elements ($\Delta C_i/C_o \times 100$; after Gómez, 2008). B. Metal contents of the polymetallic veins based on Gómez (2008) data. The polymetallic veins are located within (Cardoza mine) and surrounding (Santa Teresa, Rosarito, Carmen mines) the phyllic halo. Notice that Rosarito and Santa Teresa veins show the highest Cu content while Rosarito and Carmen veins have similar Pb–Zn–Ag contents.

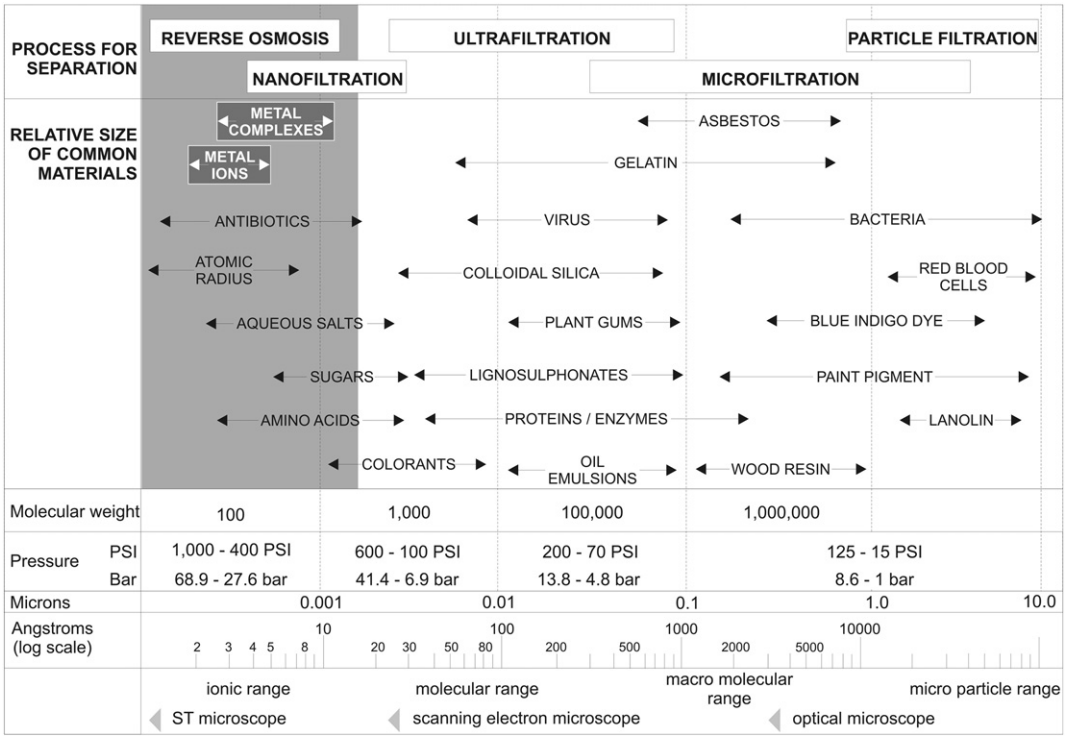

Fig. 3. Membrane separation systems and their filtration spectrum. The five considered categories are particle filtration: PF, microfiltration: MF, ultrafiltration: UF, nanofiltration: NF, and hyperfiltration/Reverse Osmosis: RO. Note that some of these categories show some degree of overlap. PF, MF and UF are size exclusion processes; NF and RO also involve ionic diffusion (NF is also known as "Selective Reverse Osmosis"). Data compiled from industry and research literature, and own calculations for metal complexes via Formula (1) in text.

Separating two solutions at different temperatures, pressures and solute concentrations, the consequent potential-energy gradient generated by this clay membrane will automatically trigger equilibrium processes: thermo-, reverse- and/or chemical-osmosis (Denbigh and Raumann, 1952; Ekbote and Abousleiman, 2003; Villaluenga et al., 2006; Fig. 4). All these osmotic-related processes involve selective transport through this clay membrane, restricting the passage of solutes through the membrane in relation to the passage of the solvent. This differential passage results in the consequent dilution of the permeate solution and the concentration of solutes on the "feed" solution side (Fig. 4).

At the *Infiernillo* deposit, pressure gradient would be consistent with fluid transport from the magmatic source outwards through the membrane, activating Reverse Osmosis (Fig. 4). Temperature gradient and presence of illite and kaolinite as hydrophobic clay minerals would have enhanced osmotic transport towards the external side of the halo (thermal-osmosis; Villaluenga et al., 2006).

5. Reverse Osmosis

As was previously mentioned, osmosis-related processes involve relative restriction or hindrance of transport of solutes through the membrane in relation to passage of the solvent. The filtration spectrum of Reverse Osmosis embraces the ionic range, so it is commonly used at environmental temperature to concentrate and separate metal ions, aqueous salts and atomic radius particles from their solvents (Hendricks, 2011; Fig. 3).

Although there is no available information about metal–complex sizes for testing Reverse Osmosis as a viable osmotic differentiation process for

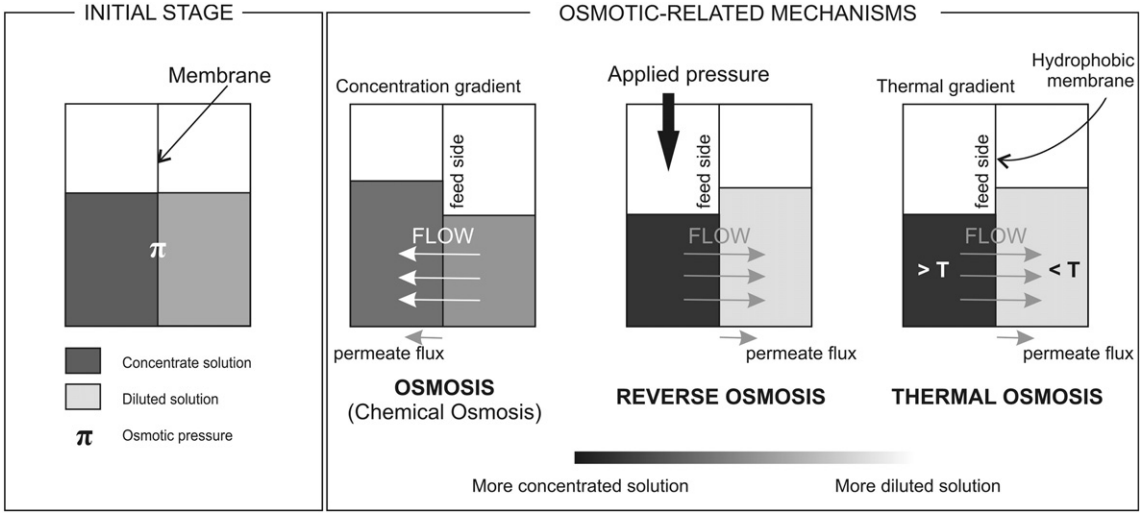

Fig. 4. Mechanisms associated with osmotic transport.

these substances, recent publications refer to removal of heavy metal ions through nanofiltration (see the overlap of Reverse Osmosis and nanofiltration fields in Fig. 3). In those cases, it is required the previous complexing of metals (Abhang et al., 2013; Lastra et al., 2004; Murthy and Chaudhari, 2009; Rogel-Hernández et al., 2006). Likewise, a rough estimation of metal–complex diameter could be obtained through the formula

$$\mathbf{R_{cx}} = \mathbf{r_{ca}} + \mathbf{2r_l} \quad (1)$$

where $\mathbf{R_{cx}}$ represents the radius of the metal–complex, $\mathbf{r_{ca}}$ is the cation radius and $\mathbf{r_l}$ corresponds to the ligand radius.

According to Formula (1) and considering for example the large Pb^{2+} cation and the large Cl^- ligand (see Table 1) this would imply a complex diameter of ca. 9.9 Å that is a favorable size for a Reverse Osmosis operating range (Fig. 3). Therefore, Reverse Osmosis does represent a reliable separation mechanism for metal-complexes as indicated in Fig. 3.

Restriction of passage of solute through a membrane is known as "membrane rejection", a measure relative to the feed concentration that indicates the amount of solute that does not pass through the membrane (Amjad et al., 1998). Rejection (R) is mathematically expressed as

$$\mathbf{R} = (\mathbf{C_f} - \mathbf{C_p})/\mathbf{C_f}, \quad (2)$$

where $\mathbf{C_f}$ and $\mathbf{C_p}$ are the concentration of solute in the feed and in the permeate flux respectively (Fig. 4). Usually rejection is expressed as R × 100 (percentage of rejection).

Different parameters are known to influence both permeate flux and passage of solutes through a Reverse Osmosis membrane, which depend on membrane and feed water characteristics (Bartels et al., 2005). Membrane-dependant factors include membrane pore size, density charge and thickness. Feed water parameters comprise pressure (net pressure and feed pressure), temperature of feed water and feed water chemistry (solute concentration, pH, etc.). Feed water parameters control Reverse Osmosis efficiency because they command solute passage ratio (Bartels et al., 2005; Filmtec, 2012). In the case of feed water pressure, the higher the net pressure the higher the volume of permeate and the lower the passage of solutes (Hawlader et al., 2000). Temperature of feed water also plays an important role in Reverse Osmosis efficiency because at higher temperatures, solute passage and permeate flow increase while the required operating pressure to produce flow is lower (Al-Mutaz and Al-Ghunaimi, 2001; Emalsa, 2007; Hawlader et al., 2000). Considering feed water concentration, a higher concentration increases the required feed pressure to activate Reverse Osmosis (Filmtec, 2012). In the case of solute ions, size and charge also affect the passage because the larger the size and the larger the charge, the higher the rejection (or the lower the passage; e.g., Liu, 2007). Although not yet entirely understood, passage seems to be dependant on the charge/mass ratio as it shows a remarkable coincidence with the measured rejection series for metal ions (Fig. 5).

Membrane processes have received considerable attention regarding the separation and concentration of inorganic and organic substances from waste water at 25 °C and, consequently, there is a lot of information about membrane rejection values for this temperature for different membranes. Considering these known rejection values for 25 °C and taken into account that solute passage increases ~2%–3% per °C (Emalsa, 2007; Wilf, 2008) or slightly less (Hawlader et al., 2000) the following formula allows calculation of solute passage values for different temperatures:

$$\mathbf{SP_T} = [\mathbf{1} + (\mathbf{SPi}/\mathbf{100})]^{\mathbf{\Delta T}} \times (\mathbf{100} - \mathbf{R_o}) \quad (3)$$

where $\mathbf{SP_T}$ represents the solute passage value for a given temperature T; **SPi** corresponds to the solute passage increase per °C; $(\mathbf{100} - \mathbf{R_o})$ refers to SP_o, that is the reference solute passage value at 25 °C ($SP_{25\ °C}$); and **ΔT**, the difference between T and the reference temperature of 25 °C.

Because no data were found about the precise membrane rejection value concerning the specific clays that resulted from phyllic alteration at the *Infiernillo* deposit, a rejection-value span was calculated through the available maximum and minimum rejection values for different membranes. The calculated SP_T value ranges for different temperatures considering the different temperature correction factors (2% and 1.5% per °C) are shown in Table 2 and Fig. 6. In spite of the fact that some solutes show some degree of overlap in SP_T intervals (Table 2 and Fig. 6), it must be emphasized here that they have to follow the same relative rejection (/passage) relationship that is shown in Fig. 5A.

a) Considering an incremental rate of 2% per °C for Formula (3) and a passage-value range obtained from membrane literature, Ag and Pb could reach the highest fugacity (100% passage) at temperatures of ≥141 °C when Cu, Zn and Fe would be only partially leaked (Cu/Zn/

Table 1
Approximated size of some simple ligands and cations that are significant in porphyry type systems (Å: Angstrom).

Ligand	Ionic radius (Å)	Cation	Ionic radius (Å)
OH^-	1.10	Fe^{3+}	0.67
NO^{2-}	1.30	Cu^{2+}	0.72
F^-	1.33	Fe^{2+}	0.82
O^{2-}	1.40	Zn^{2+}	0.83
H_2O	1.40	Pb^{4+}	0.84
Cl^-	1.81	Ag^{2+}	0.89
S^{2-}	1.84	Cu^+	0.96
Br^-	1.95	Ag^+	1.13
I^-	2.20	Pb^{2+}	1.32

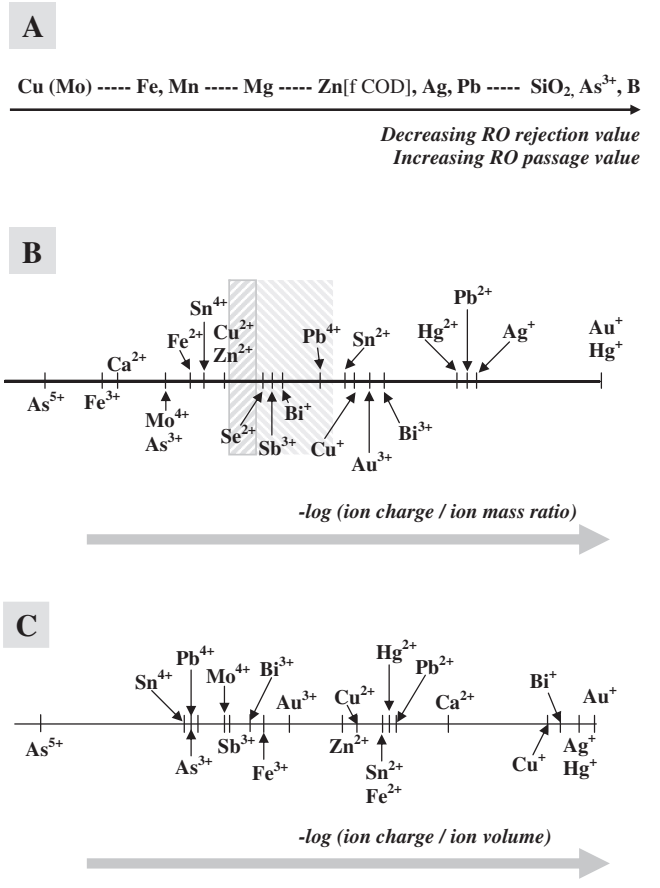

Fig. 5. Empiric correspondence between available ion rejection (/passage) values and ion charge/weight and ion charge/volume ratios. A. Metal ion rejection (/passage) value series based on compiled industry and research data. COD: Chemical Oxygen Demand. B. Calculated metal ion charge/mass series. Shadow areas divide more rejected from more mobile metal ions, leading to the observed metal partitioning in the *Infiernillo* deposit. C. Calculated metal ion charge density (charge/volume) series. Note the stronger correspondence between series A and B than A and C.

Table 2
Solute passage calculated for different temperatures for Reverse Osmosis. Intervals of passage value for some ions (minimum SP_T — maximum SP_T) at temperatures ranging from 25 °C to 250 °C considering a correction factor of 2% per °C (A, B) and from 25 °C to 325 °C considering a correction factor of 1.5% per °C (C). Intervals, not specific values, are considered because $SP_{25\ °C}$ values depend on membrane characteristics and there is no information about rejection of *Infiernillo*'s clay case (rejection would be inside the wide range of membranes that were considered). Table 2A comprises the ranges calculated from all the $SP_{25\ °C}$ values obtained in the specific literature (see Fig. 6A), whereas ranges from Table 2B resulted considering the most common $SP_{25\ °C}$ value ranges (see Fig. 6B) and Table 2C consists of the results based on the most common $SP_{25\ °C}$ value ranges together with a correction factor of 1.5% per °C (see Fig. 6C). Dark gray cells refer the occurrence of 100% of solute passage; light gray cells indicate the range where total solute passage is probable but depending on membrane nature; white cells denote partial passage (inability for total solute passage). Note that at low temperature, ions are retained by the membrane whereas at temperatures higher than 260 °C (correction factor 2% per °C) and 325 °C (correction factor 1.5% per °C), membrane do not retain any ionic species.

a

2% per ºC

Range SP_T values — **Limit T ~ 260ºC (higher T for total passage)**

T	ΔT	$(1.02)^{\Delta T}$	PASSAGE % (= 100% - REJECTION %) SP_T						
			Ag^+	Cu^{2+}	SiO_2	Fe	Zn	Pb	As^{3+}
25ºC	0ºC	1	2-10	1-7	5-20	1-8	1-7	2-7	4-30
50ºC	25ºC	1.64	3.28-16.4	1.64-11-48	8.20-32.80	1.64-13.12	1.64-11-48	3.28-11.48	6.56-49.20
75ºC	50ºC	2.69	5.38-26.9	2.69-18.83	13.45-53.80	2.69-21.52	2.69-18.83	5.38-18.83	10.76-80.70
100ºC	75ºC	4.41	8.82-44.1	4.41-30.87	22.05-88.20	4.41-35.28	4.41-30.87	8.82-30.87	17.64->100
125ºC	100ºC	7.24	14.48-72.4	7.24-50.68	36.2->100	7.24-57.92	7.24-50.68	14.48-50.68	28.96->100
150ºC	125ºC	11.88	23.76->100	11.88-83.16	59.4->100	11.88-95.04	11.88-83.16	23.76-83.16	47.52->100
175ºC	150ºC	19.50	39.00->100	19.50->100	97.5->100	19.50->100	19.50->100	39.00->100	78.00->100
200ºC	175ºC	31.99	63.98->100	31.99->100	>100	31.99->100	31.99->100	63.98->100	>100
225ºC	200ºC	52.48	>100	52.48->100		52.48->100	52.48->100	>100	
250ºC	225ºC	86.10		86.10->100		86.10->100	86.10->100		
275ºC	250ºC	141.26		>100		>100	>100		

b

2% per ºC

Common range SP_T values — **Limit T ~ 260ºC (higher T for total passage)**

T	ΔT	$(1.02)^{\Delta T}$	PASSAGE % (= 100% - REJECTION %) SP_T						
			Ag^+	Cu^{2+}	SiO_2	Fe	Zn	Pb	As^{3+}
25ºC	0ºC	1	3-5	1-4	10-15	1-2	2-4	2-6	5-10
50ºC	25ºC	1.64	4.92-8.20	1.64-6.56	16.40-24.60	1.64-3.28	3.28-6.56	3.28-9.84	8.20-16.40
75ºC	50ºC	2.69	8.07-13.45	2.69-10.76	26.90-40.35	2.69-5.38	5.38-10.76	5.38-16.14	13.45-26.90
100ºC	75ºC	4.41	13.23-22.05	4.41-17.64	44.10-66.15	4.41-8.82	8.82-17.64	8.82-26.46	22.05-44.10
125ºC	100ºC	7.24	21.72-36.20	7.24-28.96	72.40->100	7.24-14.48	14.48-28.96	14.48-43.44	36.20-72.40
150ºC	125ºC	11.88	35.64-59.40	11.88-47.52	>100	11.88-23.76	23.76-47.52	23.76-71.28	59.40->100
175ºC	150ºC	19.50	58.50-97.50	19.50-78.00		19.50-39.00	39.00-78.00	39.00->100	97.50->100
200ºC	175ºC	31.99	95.97->100	31.99->100		31.99-63.98	63.98->100	63.98>100	>100
225ºC	200ºC	52.48	>100	52.48->100		52.48->100	>100	>100	
250ºC	225ºC	86.10		86.10->100		86.10->100			
275ºC	250ºC	141.26		>100		>100			

Fe $SP_{141\ °C}$ = 10–70%; Table 2A and reference bar IV in Fig. 6A). Calculations show that SiO_2 and As^{3+} cannot be retained by any membrane at ~180 °C, and that at this temperature Ag/Pb and Cu/Zn would be respectively leaked out by 43–100% and 22–100% (Table 2A and reference bar III in Fig. 6A). At 225 °C, membrane passage for Cu and Zn will be 53–100% whereas for Ag and Pb it will be 100% (Table 2A and reference bar II in Fig. 6A). Calculations would indicate that under the selected $SP_{25\ °C}$-value ranges and the considered 2% per °C correction factor, no membrane effects were expected at more than 260 °C, and all considered solutes would go through the membrane (Table 2A and reference open bar I in Fig. 6A). The calculated passage values reveal that higher temperatures enhance rejection contrast between different metal ions, leading to an osmotic differentiation phenomenon (Fig. 6). These indicate that osmosis-related differentiation would be more effective at temperatures that are consistent with the phyllic stage of the *Infiernillo* deposit hydrothermal system.

b) Solute passage values were recalculated constraining the $SP_{25\ °C}$ intervals for different membranes into the most common $SP_{25\ °C}$-values and maintaining the correction factor of 2% per °C. Results are shown in Table 2B and the representative curves are presented in Fig. 6B. Considering a temperature of ~141 °C (Table 2B and reference bar IV in Fig. 6B), SiO_2 will pass through the membrane while As^{3+}

Table 2 (*continued*)

c

1.5 % per °C

Common range SP_T values — **Limit T ~ 325°C (higher T for total passage)**

T	ΔT	$(1.015)^{\Delta T}$	*PASSAGE % (= 100% - REJECTION %) SP_T*						
			Ag^+	Cu^{2+}	SiO_2	Fe	Zn	Pb	As^{3+}
25°C	0°C	1	3-5	1-4	10-15	1-2	2-4	2-6	5-10
50°C	25°C	1.45	4.35-7.25	1.45-5.80	14.50-21.75	1.45-2.90	2.90-5.80	2.90-17.40	7.25-14.50
75°C	50°C	2.10	6.30-10.50	2.10-8.40	21.00-31.50	2.10-4.20	4.20-8.40	4.20-25.2	10.50-21.00
100°C	75°C	3.05	9.15-15,25	3.05-12.20	30.50-45.75	3.05-6.10	6.10-12.20	6.10-36.6	15.25-30.50
125°C	100°C	4.43	13.29-22.15	4.43-17.72	44.30-66.45	4.43-8.86	8.86-17.72	8.86-53.16	22.15-44.30
150°C	125°C	6.43	19.29-32.15	6.43-25.72	64.30-96.45	6.43-12.86	12.86-25.72	12.86-77.16	32.15-64.30
175°C	150°C	9.33	27.99-46.65	9.33-37.32	93.30->100	9.33-18.66	18.66-37.32	18.66->100	46.65-93.30
200°C	175°C	13.53	40.59-67.65	13.53-54.12		13.53-27.06	27.06-54.12	27.06->100	67.65->100
225°C	200°C	19.64	58.92-98.20	19.64-78.56		19.64-39.28	39.28-78.56	39.28->100	98.20->100
250°C	225°C	28.50	85.50->100	28.50->100		28.50-57.00	57.00->100	57.00->100	
275°C	250°C	41.35		41.35->100	>100	41.35-82.70	82.70->100	82.70->100	
300°C	275°C	60.00	>100	60.00->100		60.00->100			>100
325°C	300°C	87.10		87.10->100		87.10->100	>100	>100	
350°C	325°C	126.32		>100		>100			

could be partially or entirely removed depending on the membrane characteristics. On the other hand, Ag, Pb, Cu, Zn and Fe will be predominantly retained on the membrane feed side. At ~180 °C, SiO_2 and As^{3+} will be removed, Ag and Pb could be also removed depending on the membrane type, while Cu, Zn and Fe will be the most retained solutes (reference bar III in Fig. 6B). At ~205 °C (reference bar II in Fig. 6B), Fe will be the only one strongly rejected solute. As in case a), case b) show the same ~260 °C maximum temperature constraining the existence of osmosis-related differentiation (Table 2B and reference open bar I in Fig. 6B).

c) SP_T ranges could be adjusted when using the most common $SP_{25\ °C}$ values for different membranes and a correction factor of 1.5% per °C (Table 2C and Fig. 6C), since according to Hawlader et al. (2000) solute passage increase per °C is slightly less than 2%. Considering the same relative behavior of solutes as in case b), temperature conditions will be ~180 °C (IV in Fig. 6C), 230 °C (III in Fig. 6C) and ~265 °C (II in Fig. 6C). Applying this correction factor of 1.5% per °C, the thermal range for osmosis-related differentiation expands until 325 °C (Table 2C and reference open bar I in Fig. 6C) that is also coincident with temperature conditions during the phyllic stage. Comparisons between case b) and case c) indicate that a correction factor of 1.5% per °C broadens the temperature interval for an osmotic differentiation mechanism (150 °C–325 °C), and also it amplifies the osmotic differentiation range of solutes (see top bars for each solute in Fig. 6B and C).

6. Discussion

6.1. Reverse Osmosis and the Infiernillo deposit

6.1.1. Reverse Osmosis and the Infiernillo phyllic stage conditions

In the previous section it was mathematically demonstrated that the temperature for total metal passage during Reverse Osmosis would be constrained between 260 °C and 325 °C, depending on the used correction factor.

Fluid inclusion data for the *Infiernillo* phyllic stage indicate temperatures between 335 °C and 210 °C (Korzeniewski, 2012) enabling Reverse Osmosis to occur. This is in agreement with experimental data concerning maximum illite formation temperature (ca. 325 °C, Cathelineau, 1988; ca. 360 °C, e.g., Rosenberg, 2002). On the other hand, theoretical maximum stability temperatures for kaolinite (~250 °C, e.g., Essene and Peacor, 1995) would also support favorable conditions for Reverse Osmosis filtration but at lower temperatures (as will be considered in Section 6.1.4).

The presence of chalcopyrite in the *Infiernillo* polymetallic veins indicates that this ore-mineral should have been precipitated at temperatures lower than 335 °C, enabling its selective filtration through a Reverse Osmosis mechanism. Furthermore, experimental precipitation temperatures lower than 300 °C were also referred for chalcopyrite, depending on pH, dilution and chemical reduction (e.g., 300–200 °C at pH ~ 5; Reed and Palandri, 2006), as well as on a_{Cl^-}, and oxygen fugacity (see Xiao et al., 1998).

6.1.2. Reverse Osmosis and metal zoning at the phyllic stage

Reverse Osmosis passage values (SP_T) for Cu are lower than for Ag and Pb (Figs. 5 and 6), which explains why copper is concentrating at the inner side of the phyllic halo (Figs. 1C and 7A), acting as a sieve for copper. Moreover, when a clay membrane rejects partially the solute, a concentration–polarization-layer (CPL) forms at the higher-pressure interface of the membrane. On this feed side of the membrane, solute concentration would exceed the solute concentration in the bulk solution by about 13–20% (Filmtec, 2012) and consequently, Cu concentration, nearest to the membrane, may reach supersaturation leading to ore metal precipitation (DeRosa et al., 1997; Whitworth and DeRosa, 1997). On the other hand, the more osmotically mobile Pb, Ag, and Zn ions would be relatively more abundant in the permeate fluid, so base metals would preferentially concentrate in the polymetallic veins

instead of being disseminated in the phyllic halo (Fig. 7A). Therefore Ag, Zn and Pb-bearing solutes would be separated from the osmotically-induced flow out of the halo, where: a) they precipitate in the polymetallic veins due to the temperature–pressure drop in this area, and/or b) they achieve supersaturation in the vein-precursor fractures due to a second Reverse Osmosis filtration controlled by the phyllic alteration of the vein walls that would have also operated as a membrane. Considering the latter case b), the expected temperature declination might have resulted in a decrease in ion solute passage (Fig. 6) and consequent supersaturation and base metal precipitation. This assumption would also be supported by comparisons with other Permian porphyry copper deposit (*San Pedro*) located some 100 km south of the *Infiernillo* deposit, where a phyllic halo is absent and Cu anomalies are mainly restricted to polymetallic veins with phyllic envelopes (Gómez et al., 2015).

The zinc passage is similar to that of Cu, but is strongly dependent on the Chemical Oxygen Demand of the media that is a measure of the capacity of the solvent to consume oxygen during the oxidation of inorganic chemicals (Chianese et al., 1999). While for most metals the influence of the Chemical Oxygen Demand on their passage coefficient is negligible, for Zn, the higher the Chemical Oxygen Demand of the stream the higher its passage (Chianese et al., 1999). This dependence of Zn passage to Chemical Oxygen Demand could then explain why Zn can concentrate in polymetallic veins (e.g., *Infiernillo* deposit) and/or can overprint the Cu-enriched potassic cores (see Sillitoe, 2010).

The occurrence of As in the polymetallic veins of *Infiernillo* deposit also supports an osmosis-induced process, since As^{3+} has a high osmotic fugacity (Applied Membranes, 2003; Table 2 and Figs. 5A and 6).

Since information about metal ion rejection is restricted to those present in waste water, leachate and seawater, there is no a complete dataset for all the chemical elements present in porphyry-type deposits. However, if a theoretical relationship between the degree of rejection and the charge/mass ratio is regarded (Fig. 5), Au^{+} should show the lowest rejection values whereas Au^{3+} should have a roughly similar rejection value to Cu^{+}, but lower than Cu^{2+}. Although no quantitative rejection values for Mo was found in the literature, Huxstep and Sorg (1988) refers Mo as a moderately removed ion, and therefore its osmotic rejection behavior could have been considered as similar to Cu.

The asymmetric distribution of base metal polymetallic veins, that are absent westwards and scarce eastwards from the phyllic halo, can be also explained by a Reverse Osmosis process. Reverse Osmosis membranes tend to "fouling" and "scaling" over time. A reduction of permeate flux and of the rejection capability of the membrane should be expected as a consequence of the presence of some chemicals (Fe, silica, etc.) that harm the membrane on its feed side (Fritzmann et al., 2007). Fouling refers to the damage produced by particulate matter and is mainly caused by suspended or colloidal matter; scaling involves precipitation of inorganic material caused by concentration–polarization (CPL) on the membrane surface. Some of the most important foulants are Fe, Mn, Mg, SiO_2 and Al whereas the more frequent scalants are substances with large precipitation kinetics such as $CaCO_3$, $CaSO_4$, $BaSO_4$ and SiO_2 (Freeman and Majerle, 1995; Fritzmann et al., 2007; Jarusutthirak et al., 2007). The observed gain in Si, Fe, Mg and Al around the *Infiernillo* phyllic halo can be then explained by fouling and scaling. Instead of an expected gain in Ca, depletion in this element could be interpreted as the consequence of the non-homogeneous overprint of the late carbonatization. In this context, silicification within the phyllic halo could be not only the consequence of mineral alteration during development of the halo but also the result of SiO_2 fouling during osmotic transport. Iron is a metal with large fouling power and has a strong affinity to clay minerals, suggesting that fouling could be also the reason for the worldwide occurrence of abundant pyrite in the phyllic halo in porphyry Cu deposits.

Since presence of Fe would enhance silica scaling (Freeman and Majerle, 1995; Sahachaiyunta et al., 2002), fouling and scaling could be the cause of a significant decrease in Reverse Osmosis performance of the membrane. Considering that: a) fouling is more intense at high permeation rates (Zhu and Elimelech, 1997), b) the higher the net pressure the higher the permeation rates (Al-Bastaki and Abbas, 2000), and c) net pressure is higher E–W (parallel to σ_3-direction) than N–S, then the Reverse Osmosis process offers a reasonable explanation to polymetallic vein distribution asymmetry for the *Infiernillo* deposit. Aligned following the direction of minimum stress (σ_3; Fig. 1B), the eastern and western phyllic halo sectors would have supported higher permeation rates (Fig. 7B). Consequently, fouling would have been stronger in the eastern and western than in the southern and northern sectors of the phyllic halo, causing permeation to drop and to end early. In contrast, a lower permeation rate would have allowed continuous selective transport throughout the membrane at its southern and northern edges, which are aligned with the σ_1 maximum stress direction, thus enabling the higher ore concentration in veins (Fig. 7B). Furthermore, the highest disseminated Cu anomalies detected in the southwest of the phyllic halo (Gómez and Rubinstein, 2010b) would also support this explanation.

It must be noted that, although the asymmetric and localized distribution of polymetallic veins could indicate an asymmetrical fracture connectivity (Japas et al., 2013), the remarkable coincidence between differences in those phyllic halo features described in Section 3 and differences in metal content in veins allows to conclude that Reverse Osmosis should have contributed to this asymmetry.

In summary, asymmetric ore distribution at the *Infiernillo* deposit could be satisfactorily explained by Reverse Osmosis in a differential stress field that would enhance a differentiated permeation phenomenon through the phyllic halo. This means that metal zoning would also be a pressure-sensitive process.

6.1.3. Reverse Osmosis, differential stress and stockwork features

As a typical feature from the phyllic stage (Hedenquist and Richards, 1998), the stockwork structure has developed in the *Infiernillo* deposit. As previously reported, the main characteristics of the stockwork in the *Infiernillo* deposit is its asymmetric distribution around the phyllic halo.

The origin of stockwork linked to porphyry-type deposits is still subject of much debate (Fournier, 1999; Tosdal and Richards, 2001). Analyzed in a Reverse Osmosis perspective, the development of a concentration–polarization layer (CPL favored when fluids flow perpendicular to the membrane) as well as the progressive fouling/scaling of the phyllic membrane would have induced a temporal solute concentration at the inner side of the phyllic halo (feed side of the membrane). This higher feed fluid concentration directly influenced an osmotic pressure increase (the necessary pressure that must be applied in order to stop osmosis), and consequently an increase of feed fluid pressure that triggered the hydraulic fracturing responsible for the stockwork development. Stockwork fractures were preferentially filled by the foulants/scalants substances (e.g., SiO_2, Fe), that is consistent with the presence of quartz–pyrite–illite veins overprinting the pervasive phyllic alteration. Therefore, the presence of osmotic pressure gradients around the phyllic halo, which are controlled by the differential stress field, agrees with the observed asymmetry in the stockwork distribution at the *Infiernillo* deposit.

Summarizing, Reverse Osmosis under differential tectonic stress could also explain both, the *Infiernillo* deposit stockwork as well as its asymmetrical distribution around the phyllic halo.

6.1.4. Reverse Osmosis and late porphyry stage

At the latest stage of *Infiernillo* deposit evolution, magmatic supply declined and hydrothermal fluid pressure diminished. The Reverse Osmosis system then collapsed and pure chemical osmosis occurred (top of Fig. 7B). This reversal of the Reverse-Osmosis-induced flow (referred to here as "backflow") would induce a new input of cognate and/or meteoric waters inwards the phyllic halo, assisting them to merge with residual fluids of the phyllic stage. This late fluid activity would have led to the development of the central quartz neck.

Backflow is physically equivalent to the "backwashing" of water desalination membranes. Considering that during backwashing, the flow

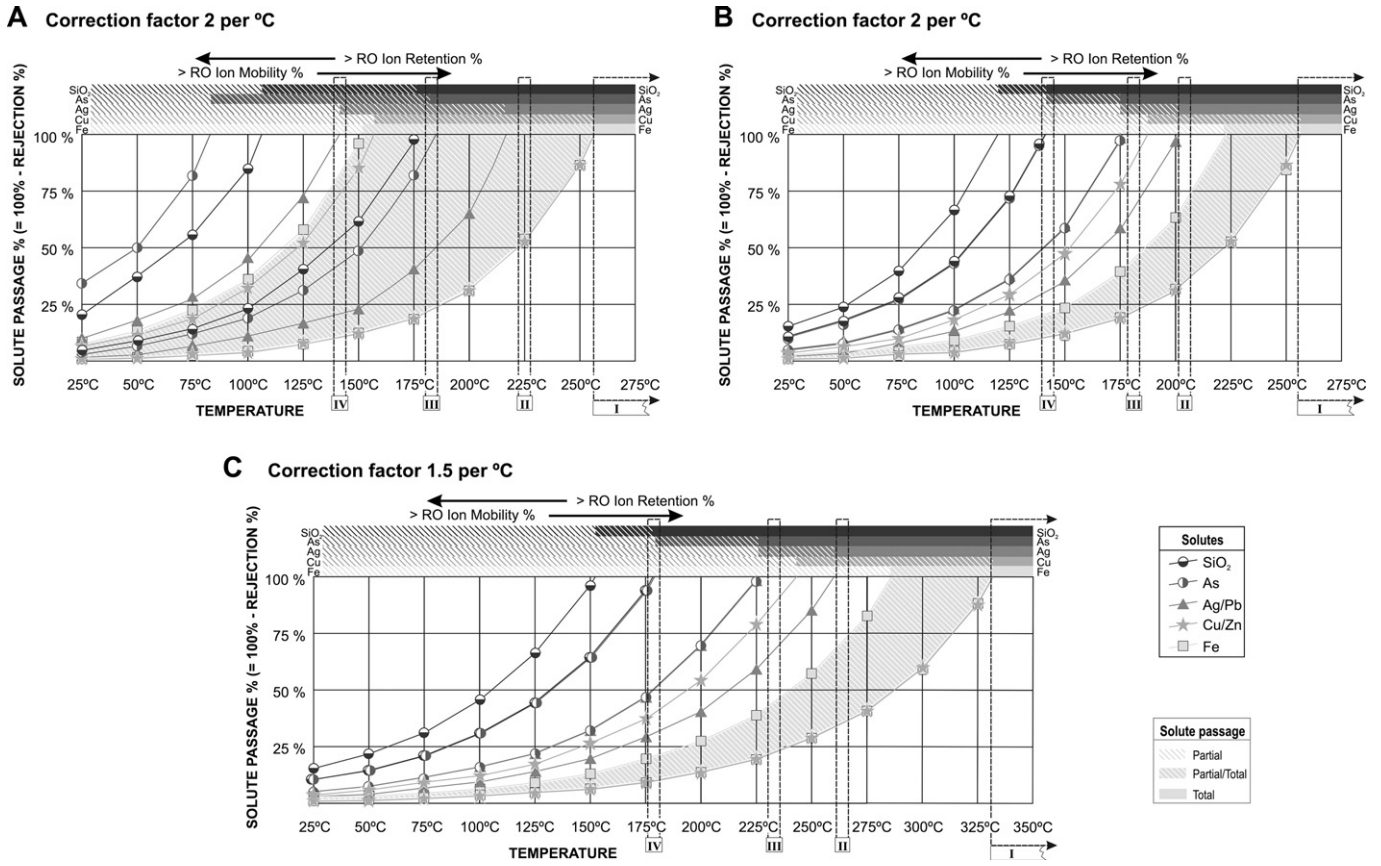

Fig. 6. Reverse Osmosis and solute passage for different temperatures. Intervals of passage values for some ion solutes (minimum SP_T — maximum SP_T) at temperatures ranging from 25 °C to 250 °C considering a correction factor of 2% per °C (A, B) and from 25 °C to 325 °C considering a correction factor of 1.5% per °C (C). Fig. 6A comprises the ranges calculated based on all the $SP_{25\ °C}$ values obtained in the specific literature, whereas Fig. 6B involves the ranges calculated based on the most common $SP_{25\ °C}$ value ranges. Fig. 6C represents the results based on the most common $SP_{25\ °C}$ value ranges together with a correction factor of 1.5% per °C. Passage value range for 25 °C for Ag (3–5), Cu (1–4), SiO_2 (10–15), Fe (1–2) and As^{3+} (5–10) were collected from available rejection data from research and industry sources. For each considered ion, the area between both curves indicates the range for probable 100% solute passage depending on the several factors described in main text (e.g., the dashed area inside the plot indicating the range for probable 100% solute passage for Fe, depending on membrane characteristics). Pb and Zn are not plotted because their similar SP_T trend to Ag. Osmotic differentiation is highlighted at the top bar. Note that i) considering a correction factor of 1.5% per °C the temperature for SP_T shifts to higher temperature and ii) no membrane effects would be observable at more than 260 °C (correction factor 2% per °C) and 325 °C (correction factor 1.5% per °C). Note that for Ag, for example, a temperature decrease would imply a change from the field of 100% Ag-passage (≥250 °C) to the field of a higher Ag retention by the membrane (<250 °C) supporting retention conditions for Ag at the polymetallic vein environment. Bars labeled, I, II, etc. refer to reference temperature analyzed and discussed in main text.

is reverted to take foulant substances out of the membrane, backflow should be then effective in removing SiO_2 and Fe into the central area of *Infiernillo* deposit. In this way, the presence of a central hydrothermal breccia composed by silicified host rock fragments cemented by hematite and low temperature SiO_2, and overprinted by late quartz–hematite veins are consistent with this Reverse Osmosis related model.

The late carbonatization process linked to the transtensional post-orogenic regime postdates the central breccia development (Gómez, 2008) constraining the time of the breccia formation to the final stages of the San Rafael orogenic phase, shortly after the transtensional regime inception. This means that this central breccia body could be formed at the time of the lowest differential stress, which is consistent with the proposed backflow scenario.

6.1.5. Reverse Osmosis and the stress environment

Infiernillo porphyry was emplaced during the final stages of the San Rafael orogenic phase (Japas et al., 2013). The structural zoning described for the *Infiernillo* deposit by Japas et al. (2013) allows to recognize a pressure gradient: dominant tectonic pressure conditions outwards the phyllic halo and magmatic pressure higher than tectonic stress inwards the phyllic halo. This pressure gradient was the trigger for Reverse Osmosis immediately after the phyllic halo developed.

Under these waning stress conditions, magmatic pressure linked to the emplacement and evolution of this deposit would be relatively strong enough to activate the pressure-sensitive Reverse Osmosis mechanism. In other words, magmatic pressure surpassing tectonic stresses would be the condition for the activation of Reverse Osmosis during the phyllic stage. Conversely, at the orogenic climax, magmatic pressure exceeding tectonic pressures is considered to be unlikely and consequently the existence of pressure gradients defined by tectonic stresses higher than magmatic pressures would not be able to trigger Reverse Osmosis. In this way, Reverse Osmosis would also explain why porphyry-type deposits are linked to declining compressional/transpressional regimes, a link previously suggested by Billa et al. (2004), Sillitoe and Hedenquist (2003), Tosdal and Richards (2001) and confirmed by Japas et al. (2013).

6.2. Reverse Osmosis linked to other porphyry deposit features

Although still speculative, Reverse Osmosis could also explain some other exceptions to the traditional model.

6.2.1. Reverse Osmosis and $\delta^{34}S_{sulfide}$ isotope zoning

The zoning pattern described by Deyell (2005) for alkalic porphyry copper deposits, with more negative $\delta^{34}S_{sulfide}$ values in the core of the deposit to more positive values outwards, would unable cooling as the main control of sulfide deposition. This author links this isotopic zoning to the progressive reduction of sulfate-rich, metal-bearing fluids outwards from the deposit core, linking zoning with redox controls.

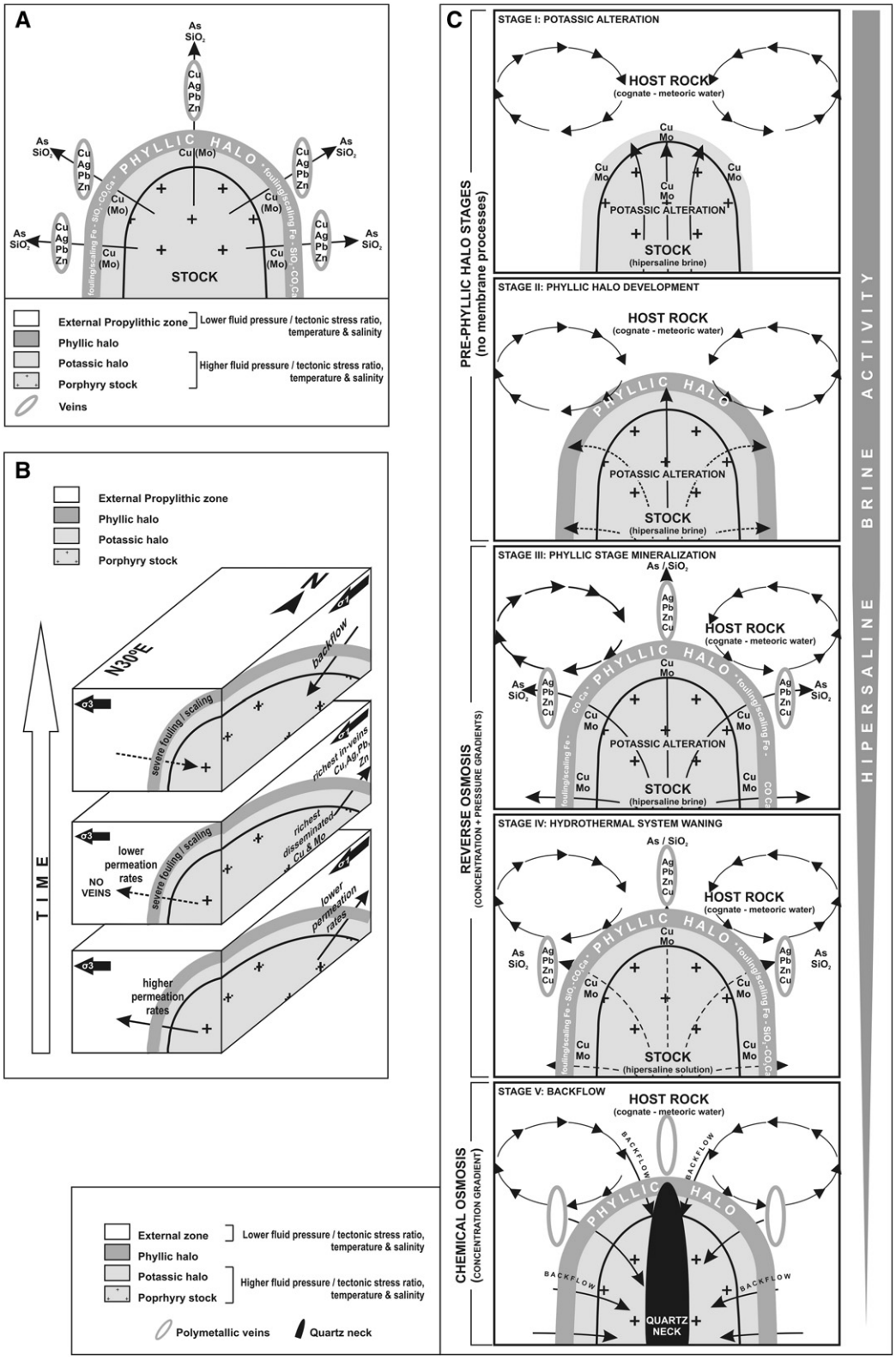

Fig. 7. Reverse Osmosis and metal zoning. A. Phyllic stage metal zoning and Reverse Osmosis. B. Incidence of differential stresses in osmotic differentiation performance. Direction of minimum stress (σ_3; see Fig. 1B) supported the highest permeation rates that resulted in strong fouling/scaling. C. Simplified sketch to show *Infiernillo* deposit evolution and particularly how Reverse Osmosis would operate in ion differentiation leading to *Infiernillo* deposit metal zoning during the phyllic stage. Stage I: Potassic alteration; Stage II: Phyllic alteration; Stage III: metal zoning overprinting controlled by Reverse Osmosis; Stage IV: Waning hydrothermal system and consequent collapse of Reverse Osmosis; Stage V: Chemical osmosis, backflow and the formation of the central hydrothermal breccia. The inception of the phyllic membrane triggers concentration (chemical)-gradients that locally modify the buoyant flow pattern leading the fluids not only to flow to the top but also towards the laterals (lateral flow).

In this context, and bearing in mind the differential solute passage imposed by the "phyllic membrane" for two different ion-solute species (sulfate and sulfide), a significant redox imbalance would have been introduced. This disproportion would have trigger redox reactions to attain equilibrium, leading to the documented $\delta^{34}S_{sulfide}$ zoning.

In summary, the early ore deposition related to the *Infiernillo* deposit began at the potassic stage, prior to the phyllic halo formation (Fig. 7C Stage I). At this time, temperature was favorable for Cu and Mo deposition. During the inception of the phyllic halo (Fig. 7C Stage II), hydrothermal fluids would have caused dissolution of early formed copper sulfides and remobilization of Cu. This late-stage alteration represented the starting point for a late overprinted metal zoning that was controlled by Reverse Osmosis (Fig. 7C Stage III). In this way, ore deposition constrained by Reverse Osmosis can overprint the mineralization of the potassic stage imposing its own metal zoning. As the hydrothermal system declined, hydrothermal pressure diminished until it equaled the osmotic pressure; at this point Reverse Osmosis stopped working (Fig. 7C Stage IV). The continuous decrease in hydrothermal fluid pressure allowed reversal of the osmotic transport (from Reverse Osmosis to chemical osmosis) leading to backflow and the consequent development of the central hydrothermal breccia (Fig. 7C Stage V). Following this model, Reverse Osmosis operating during the phyllic stage could answer a question of Sillitoe (2010) about *what controls metal depletion versus metal enrichment during chlorite–sericite and sericitic* (phyllic) *overprints*.

7. Conclusions

All the evidence pointed out above vouch for Reverse Osmosis as a geologically viable, natural, pressure-sensitive process that favors ore concentration during the phyllic stage in porphyry systems based on the existence of potential-energy gradients and different relative rejection values for different metal ions. At temperatures corresponding to those of porphyry phyllic halo formation, and in presence of a phyllic (clay) membrane, Cu, Ag, Zn and Pb would show a strong osmotic differentiation that could have led to the observed metal zoning. The viability of Reverse Osmosis would be also supported because, as a low-energy consumption and slow-process, it seems to be also compatible with geological time rates linked to porphyry evolution.

Regardless of the case of *Infiernillo* deposit, Reverse Osmosis could also explain some departures from the traditional model of porphyry evolution in other porphyry deposits. The recognition of this new physico-chemical factor controlling ore formation would benefit the knowledge of complementary processes that could operate during porphyry deposit evolution worldwide and would clarify some still unresolved questions contributing to minimization of some exploration risks.

Conflict of interest

There is no conflict of interest.

Acknowledgments

We would like to thank to M.L. Japas, M.C. Sellés, J.M. Sellés and O.M. Rabbia for the discussions concerning the physico-chemical topics of this manuscript. We are grateful to Richard Tosdal and an anonymous reviewer for their constructive and motivating reviews, as well as to the Editor Franco Pirajno for the editorial work.

References

Abhang, R.M., Wanib, K.S., Patilc, V.S., Pangarkara, B.L., Parjanea, S.B., 2013. Nanofiltration for recovery of heavy metal ions from waste water — a review. Int. J. Res. Environ. Sci. Technol. 3, 29–34.
Al-Bastaki, N.M., Abbas, A., 2000. Predicting the performance of RO membranes. Desalination 132, 181–187.
Al-Mutaz, I.S., Al-Ghunaimi, M.A., 2001. Performance of reverse osmosis units at high temperatures: IDA World Congr. Desalination and Water Reuse Proc., Bahrain, pp. 1–9.
Amjad, A., Zibrida, J.F., Zuhl, R.W., 1998. Reverse osmosis technology. fundamentals and water applications. Ann. Convention and Exposition, Assoc. Water Technol. Proc., Washington, pp. 1–18.
Applied Membranes, 2003. http://www.appliedmembranes.com.
Bartels, C., Franks, R., Rybar, S., Schierach, M., Wilf, M., 2005. The effect of feed ionic strength on salt passage through reverse osmosis membranes. Desalination 184, 185–195.
Bermúdez, A., Delpino, D., Frey, F., Saal, A., 1993. Los basaltos de retroarco extraandinos. In: Ramos, V.A. (Ed.), Geología y recursos naturales de Mendoza: Relat. 12° Congr. Geol. Argent, pp. 161–172.
Billa, M., Cassard, D., Lips, A.L.W., Bouchot, V., Tourlière, B., Stein, G., Guillou-Frottier, L., 2004. Predicting gold-rich epithermal and porphyry systems in the Central Andes with a continental-scale metallogenic GIS. Ore Geol. Rev. 25, 39–67.
Bordonaro, O., Keller, M., Lehnert, O., 1996. El Ordovícico de Ponón Trehue en la Provincia de Mendoza (Argentina): Redefiniciones estratigráficas. Congr. Geol. Argent. Abstracts, Buenos Aires 1, pp. 541–550.
Carpio, F., Mallimacci, H., Rubinstein, N., Salvarredi, J., Sepúlveda, E., Centeno, R., Rosas, M., Vargas, D., 2001. Metalogenia del Bloque de San Rafael, Mendoza. Serv. Geol. Min. Argent., Serie Contribuciones Técnicas, Recursos Minerales (109 pp.).
Cathelineau, M., 1988. Cation site occupancy in chlorites and illites as a function of temperature. Clays Clay Miner. 23, 471–485.
Chianese, A., Ranauro, R., Verdone, N., 1999. Treatment of landfill leachate by reverse osmosis. Water Res. 33, 647–652.
Cingolani, C.A., Varela, R., 1999. Rb–Sr isotopic age of basement rocks of the San Rafael Block, Mendoza, Argentina. 2° South American Symposium Isotope Geology, Extended Abstracts, pp. 23–26.
Denbigh, K.G., Raumann, G., 1952. The thermo-osmosis of gases through a membrane. I. Theoretical. Proc. R. Soc. Lond. Ser. A Math. Phys. Sci. 210, 377–387.
DeRosa, G., Whitworth, T.M., Lueth, V., 1997. Experimental evidence for potential natural remediation of heavy metal plumes. WERC/HSRC 97 Joint Conference on the Environment, Albuquerque, NM (http://earth.geo.arizona.edu/97/program/friday/08DerosaG.5.html).
Deyell, C.L., 2005. Sulphur isotope zonation at the Mt Polley alkalic porphyry Cu–Au deposit, British Columbia, Canada. In: Mao, J., Bierlein, F.P. (Eds.), Mineral Deposit Research: Meeting the Global Challenge 1.
Di Tommaso, I., Rubinstein, N.A., 2007. Hydrothermal alteration mapping using ASTER data in the Infiernillo porphyry deposit, Argentina. Ore Geol. Rev. 32, 275–290.
Ekbote, S., Abousleiman, Y., 2003. Poromechanics stability analyses for inclined wellbores under non-isothermal conditions in chemically active formations. 16th SCE Eng. Mech. Conf. Proc., Seattle, pp. 1–8.
Emalsa, 2007. Curso de Osmosis Inversa. http://www.emalsa.es/3/3_10_7.php.
Espejo, I.S., López Gamundí, O.R., 1994. Source versus depositional controls on sandstone composition on a foreland basin: El Imperial Formation (mid-Carboniferous–lower Permian) San Rafael Basin, western Argentina. J. Sediment. Res. A64, 8–16.
Essene, E.J., Peacor, D.R., 1995. Clay mineral thermometry. A critical perspective. Clays Clay Miner. 43, 540–553.
Filmtec, 2012. FILMTEC™ membranes. http://www.filmtec.com.
Fournier, R.O., 1999. Hydrothermal processes related to movement of fluid from plastic into brittle rock in the magmatic–epithermal environment. Econ. Geol. 94, 1193–1211.
Freeman, S.D.N., Majerle, R.J., 1995. Silica fouling revisited. Desalination 103, 113–115.
Fritz, S.J., 1986. Ideality of clay membranes in osmotic processes: a review. Clays Clay Miner. 34, 214–223.
Fritz, S.J., Marine, I.W., 1983. Experimental support for a predictive osmotic model of clay membranes. Geochim. Cosmochim. Acta 47, 1515–1522.
Fritzmann, C., Löwenberg, J., Wintgens, T., Melin, T., 2007. State-of-the-art of reverse osmosis desalination. Desalination 216, 1–76.
Fuschini, M., 1968. Informe final Área de Reserva No 26. Zona: Infiernillo. Plan Cordillerano. Serv. Geol. Min. Argent (33 pp.).
Garavito Rojas, A.M.F., 2006. Project: chemical osmosis in clayey sediments. Field experiments and numerical modelling. http://www.onderzoekinformatie.nl/nl/oi/nod/onderzoek/OND1303638/.
Gargiulo, M.F., Rubinstein, N.A., Carpio, F., Salvarredi, J., 2007. Caracterización de la zona de alteración Central II, Bloque San Rafael, provincia de Mendoza. Rev. Asoc. Geol. Argent. 62, 387–395.
Gómez, A., 2008. Geología del Deposito el Infiernillo, Bloque de San Rafael, Mendoza. (Unpublished M.Sc. thesis). Universidad de Buenos Aires, Buenos Aires.
Gómez, A., Rubinstein, N., 2010a. Caracterización genética del distrito minero El Infiernillo, Bloque de San Rafael, provincia de Mendoza. Rev. Asoc. Geol. Argent. 67, 231–238.
Gómez, A., Rubinstein, N., 2010b. Geology of San Pedro Mining District, San Rafael Massif, Argentina. Int. Geol. Congr. S. Hemisph. (GEOSUR): Boll. Geof. Teor. Aplic, pp. 236–239.
Gómez, A., Rubinstein, N., Valencia, V., 2015. Gondwanan magmatism with adakite-like signature linked to Cu (Mo)-porphyry deposits from the San Rafael Massif, Mendoza province, Argentina. Chem. Erde 75, 89–104.
Gustafson, L.B., Hunt, J.P., 1975. The porphyry copper deposit at El Salvador Chile. Econ. Geol. 70, 857–912.
Hart, M., 2012. Low-head hyperfiltration through Jurassic–Cretaceous metamorphic Darrington Phyllite discs (from the Northwest Cascades of Washington State, USA). Hydrogeol. J. http://dx.doi.org/10.1007/s10040-012-0905-8.
Hawlader, M.N.A., Ho, J.C., Chua, K.T., 2000. Desalination of seawater: an experiment with RO membranes. Desalination 132, 275–280.
Hedenquist, J.W., Richards, J., 1998. The influence of geochemical techniques on the development of genetic models for porphyry copper deposits. In: Richards, J.P., Larson, P.B. (Eds.), Reviews in Economic Geology 10. Soc. Econ. Geol. Inc., pp. 235–256.
Hendricks, D., 2011. Fundamentals of Water Treatment Unit Processes. CRC Press, Boca Raton (884 pp.).

Huxstep, M.R., Sorg, T.J., 1988. Reverse osmosis treatment to remove inorganic contaminants from drinking water. Project summary of the United States Environmental Protection Agency, Research and, Development, EPA/600/S2-87/109.
Japas, M.S., Rubinstein, N.A., Kleiman, L.E., 2013. Strain fabric analysis applied to hydrothermal ore deposits emplaced during changing geodynamical conditions (Infiernillo and Las Picazas, San Rafael Massif, Argentina). Ore Geol. Rev. 53, 357–372.
Jarusutthirak, Ch., Mattaraj, S., Jiraratananon, R., 2007. Influence of inorganic scalants and natural organic matter on nanofiltration membrane fouling. J. Membr. Sci. 287, 138–145.
Kleiman, L.E., Japas, M.S., 2009. The Choiyoi volcanic province at 34–36°S (San Rafael, Mendoza, Argentina): implications for the late Palaeozoic evolution of the southwestern margin of Gondwana. Tectonophysics 473, 283–299. http://dx.doi.org/10.1016/j.tecto.2009.02.046.
Kleiman, L.E., Salvarredi, J.A., 2001. Petrología, geoquímica e implicancias tectónicas del volcanismo triásico (Formación Puesto Viejo), bloque de San Rafael, Mendoza. Rev. Asoc. Geol. Argent. 56, 559–570.
Korzeniewski, I., 2012. Inclusiones fluidas. In: Rubinstein, N.A. (Ed.), Inst. Geol. Recur. Miner., Serv. Geol. Min. Argent. Serie Contribuciones Técnicas, Recursos Minerales 35, pp. 31–36.
Lastra, A., Gómez, D., Romero, J., Francisco, J.L., Luque, S., Álvarez, J.R., 2004. Removal of metal complexes by nanofiltration in a TCF pulp mill: technical and economic feasibility. J. Membr. Sci. 242, 97–105.
Liu, S.X., 2007. Food and Agricultural Wastewater Utilization and Treatment. Blackwell Publishing.
Llambías, E.J., Kleiman, L.E., Salvarredi, J.A., 1993. Magmatismo gondwánico de Mendoza. In: Ramos, V.A. (Ed.), Geología y Recursos Naturales de Mendoza: Relat. 13° Congr. Geol. Argent, pp. 53–64.
Lowell, J.D., Gilbert, J.M., 1970. Lateral and vertical alteration mineralization zoning in porphyry ore deposits. Econ. Geol. 65, 373–408.
MacKay, R.A., 1946. The control of impounding structures on ore deposition. Econ. Geol. 41, 13–46.
Marine, I.W., Fritz, S.J., 1978. Osmotic model to explain anomalous heads. Ann. Meet. Conf. Geol. Soc. Am. Proc., Toronto, pp. 1–30.
Murthy, Z.V.P., Chaudhari, L.B., 2009. Separation of binary heavy metals from aqueous solutions by nanofiltration and characterization of the membrane using Spiegler–Kedem model. Chem. Eng. J. 150, 181–187.
Pirajno, F., 2009. Hydrothermal Processes and Mineral Systems. Springer-Verlag (1250 pp.).
Reed, M.H., Palandri, J., 2006. Sulfide mineral precipitation from hydrothermal fluids. Rev. Mineral. Geochem. 61, 609–631.
Rocha-Campos, A.C., Basei, M.A., Nutman, A.P., Kleiman, L.E., Varela, R., Llambías, E., Canile, F.M., da Rosa, O.C.R., 2011. 30 million years of Permian volcanism recorded in the Choiyoi igneous province (W Argentina) and their source for younger ash fall deposits in the Paraná Basin: SHRIMP U–Pb zircon geochronology evidence. Gondwana Res. 19, 509–523.
Rogel-Hernández, E., Espinoza-Gómez, H., Lin, S.W., Ames, A., García, C., Ramos, R., 2006. Remoción de Ca^{2+}, Fe^{2+}, Pb^{2+}, empleando una electrocelda de membranas de ultrafiltración. 5° Congr. Internac. y 11° Congr. Nac. Cs. Ambient (http://www.uaemex.mx/Red_Ambientales/docs/memorias/Extenso/TA/EC/TAC-47.pdf).
Rosenberg, P.E., 2002. The nature, formation, and stability of end-member illite: a hypothesis. Am. Mineral. 87, 103–107.
Rubinstein, N.A., Gargiulo, M.F., 2005. Análisis textural de cuarzo hidrotermal del depósito El Pantanito, provincia de Mendoza: nuevos aportes sobre su génesis. Rev. Asoc. Geol. Argent. 60, 96–103.
Rubinstein, N.A., Carpio, F., Mallimacci, H., 2000. La zona de alteración Las Chilcas, provincia de Mendoza. Congr. Miner. Metalog., Argentina, pp. 454–456.
Rubinstein, N.A., Ostera, H., Mallimacci, H.S., Carpio, F., 2004. Lead isotopes from Gondwanic ore polymetallic vein deposits, San Rafael Massif, Argentina. J. S. Am. Earth Sci. 16, 595–602.
Rubinstein, N.A., Gómez, A., Mallimacci, H., 2012. La zona de alteración Arroyo La Chilca-Zanjón del Buitre, bloque de San Rafael, Mendoza. Rev. Asoc. Geol. Argent. 69, 287–295.
Rubinstein, N.A., Gómez, A., Kleiman, L.E., 2013. Caracterización litofacial y geoquímica de las volcanitas del área del Distrito Minero el Infiernillo. Rev. Asoc. Geol. Argent. 70, 394–401.
Sahachaiyunta, P., Koo, T., Sheikholeslami, R., 2002. Effect of several inorganic species on silica fouling in RO membranes. Desalination 144, 373–378.
Sillitoe, R.H., 2010. Porphyry copper systems. Econ. Geol. 105, 3–41.
Sillitoe, R.H., Hedenquist, J.W., 2003. Linkages between volcanotectonic settings, orefluid compositions, and epithermal precious-metal deposits. Soc. Econ. Geol. Spec. Publ. 10, 315–343.
Spirakis, Ch., 1977. The role of semipermeable membranes in the Formation of Certain Vanadium–Uranium deposits. Econ. Geol. 72, 1442–1448.
Tosdal, R.M., Richards, J.P., 2001. Magmatic and structural controls on the development of porphyry Cu ± Mo ± Au deposits. In: Richards, J.P., Tosdal, R.M. (Eds.), Structural controls on ore deposits. Rev. Econ. Geol. 14, pp. 157–181.
Villaluenga, J.P.G., Seoane, B., Barragán, V.M., Ruiz-Bauzá, C., 2006. Thermo-osmosis of mixtures of water and methanol through a Nafion membrane. J. Membr. Sci. 274, 116–122.
Whitworth, T.M., DeRosa, G., 1997. Geologic membrane controls on saturated zone heavy metal transport. New Mexico Water Resources Research Institute, Technical Completion Report 1423923 (79 pp.).
Wilf, M., 2008. Membrane Types and Factors Affecting Membrane Performance. Advanced Membrane Technologies (http://www.stanford.edu/group/ees/rows/presentations/Wilf.pdf).
Xiao, Z., Gammons, C.H., Williams-Jones, A.E., 1998. Experimental study of copper(I) chloride complexing in hydrothermal solutions at 40 to 300 °C and saturated water vapor pressure. Geochim. Cosmochim. Acta 62, 2949–2964.
Zhu, X., Elimelech, M., 1997. Colloidal fouling of reverse osmosis membranes: measurements and fouling mechanisms. Environ. Sci. Technol. 31, 3654–3662.